An Analytical Approach to Single Scattering for Anisotropic Media and Light Distributions

Vincent Pegoraro [1]   Mathias Schott [1]   Steven G. Parker [1,2]

[1] University of Utah   [2] NVIDIA Corporation

ABSTRACT

Despite their numerous applications, efficiently rendering participating media remains a challenging task due to the intricacy of the radiative transport equation. While numerical techniques remain the method of choice for addressing complex problems, a closed-form solution to the air-light integral in optically thin isotropic media was recently derived. In this paper, we extend this work and present a novel analytical approach to single scattering from point light sources in homogeneous media. We propose a combined formulation of the air-light integral which allows both anisotropic phase functions and light distributions to be adequately handled. The technique relies neither on precomputation nor on storage, and we provide a robust and efficient implementation allowing for an explicit control on the accuracy of the results. Finally, the performance characteristics of the method on graphics hardware are evaluated and demonstrate its suitability to real-time applications.

Index Terms: I.3.7 [Computer Graphics]: Three-Dimensional Graphics and Realism—Color, shading, shadowing, and texture

1   INTRODUCTION

Participating media are used to model a wide variety of elements and the ability to faithfully reproduce and predict their characteristics has many scientific applications. Although realistic rendering is often of concern to the movie and gaming industries, such interest also emerged in industrial design and safety-oriented research where typical scenarios entail predicting the visibility of traffic signs in a foggy weather or exit signs in a smoke-filled room.

However, efficiently simulating accurate light transport in such media remains a challenging task due to the intricacy of the equation governing radiative energy transfer. While numerical methods such as Monte-Carlo and finite element techniques made complex problems tractable, analytical approaches to solving the air-light integral in optically thin media recently received some attention in the graphics community and showed to be a promising alternative to traditional ray-marching/slice-based volume rendering techniques.

Building on the concepts introduced in [15], this paper extends that work by considering the light distribution of anisotropic sources and provides a novel complementary reformulation of the single-scattering air-light integral as to yield a more robust evaluation scheme via domain partitioning. In addition, a more efficient and numerically stable implementation is provided, allowing interactive performance to be achieved on graphics hardware.

This document starts by providing an overview of the related work and theoretical background on the air-light integral. The derivation of the analytical reformulations as well as a practical implementation are then presented followed by some results along with a discussion of the potential limitations of the method.

2   RELATED WORK

Several techniques have been proposed in the computer graphics literature for rendering participating media, ranging from computationally expensive detailed simulations of multiple scattering in complex environments to drastic approximations primarily concerned with interactivity. [5] provides a survey of these methods.

Optically thin media were first investigated by Blinn [4] who introduced an analytical model for homogeneous media assuming an infinitely distant light source and viewer. Later, Max [12] proposed to evaluate the air-light integral by fitting Hermite cubic polynomials on adaptively subdivided intervals along the ray.

Despite the conceptual simplicity of single scattering in a homogeneous medium, numerical methods provide a convenient means of dealing with the actual complexity of the corresponding integrand and many techniques based on ray-marching [14, 8] or volume-slicing [6, 7, 10] have consequently been developed. Although simple and practical, these techniques are essentially based on Riemann sums inherently prompt to under-sampling artifacts.

Besides the image post-processing technique of Mitchell [13], several analytical approaches have also been proposed. Concerned with flight simulators, Willis [19] presented a simple model for homogeneous media solely considering a constant in-scattering term. Hoffman et al. [9] and Riley et al. [16] derived such models for single atmospheric scattering of directional sun light in constant and exponentially decreasing medium densities respectively. Considering point light sources in homogeneous media, Lecocq et al. [11] presented an angular formulation of the radiative transport equation. The resulting integrand is expanded into a Taylor series allowing each term of the polynomial to be analytically integrated for isotropic light sources while relying on numerical precomputation for anisotropic distributions. Biri et al. [3, 2] subsequently combined this angular formulation with volumetric shadows by expressing the ray integral as a difference of contributions along each segment. In their paper, Sun et al. [18] rederive Lecocq's formulation using a different notation and perform an additional linear change of variable to simplify it further. The integral is then tabulated via numerical precomputation and cheaply interpolated on the GPU during rendering. Besides trading computation for storage, the second degree of freedom of this 2D table is a distance coordinate of which the extent might not be known in advance. Wyman et al. [20] subsequently combined this approach with ray-marching as to handle light-shafts and anisotropic light distributions.

Recently, Pegoraro et al. [15] derived a closed-form solution to the air-light integral in isotropic media and extended their result to anisotropic phase functions. Although the potential of the method for accuracy over previous numerical and analytical methods was demonstrated, several limitations remain such as the restriction to isotropic light sources and the slow convergence of the Taylor series representation of the phase function over the semi-infinite subset of the new space of integration. Moreover, the evaluation of the integral exhibits a loss of efficiency as the optical thickness of the medium increases eventually leading to numerical instabilities, and a CPU implementation was solely considered. Building on the concepts introduced by the authors, this paper extends their work by addressing the various aforementioned limitations.

3 AN ANALYTICAL APPROACH TO SINGLE SCATTERING

This section starts by describing the mathematical formulation of the air-light integral in homogeneous participating media under the assumption of an anisotropic phase function and light distribution. After simplification, two analytical reformulations are subsequently derived, each yielding a bounded-to-unity and unbounded magnitude of the variable of integration over complementary intervals of the domain. In order to yield rapid convergence of the Taylor expansions with only a few terms, the combined model exploiting each reformulation over its bounded semi-interval is finally presented.
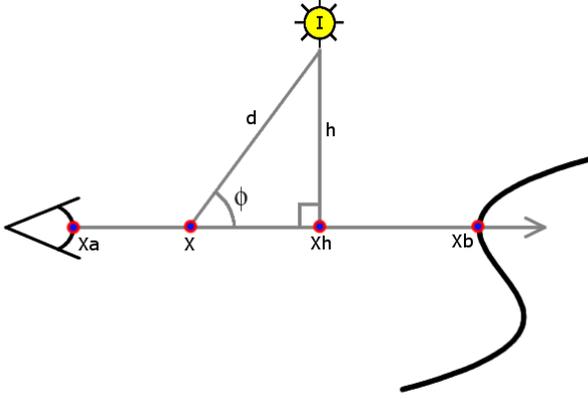
3.1 Air-Light Integral

Figure 1: Illustration of the terms involved in the computation of the air-light integral.

For a given wavelength, the radiative transport equation (RTE) describes the change of radiance L at position x along a ray of direction $\vec{\omega}$ through a medium as [17]

$$
\frac{\partial L(x,\vec{\omega})}{\partial x} = \kappa_a(x)(L_e(x,\vec{\omega}) - L(x,\vec{\omega})) + \\
\kappa_s(x)(L_i(x,\vec{\omega}) - L(x,\vec{\omega})), \tag{1}
$$

where κ_a is the absorption coefficient, κ_s the scattering coefficient, L_e the emitted radiance, and L_i the in-scattered radiance. Defining the boundary condition as the background radiance L_b formalized in equation 7, the medium radiance as L_m, the extinction coefficient as $\kappa_t = \kappa_a + \kappa_s$ and the optical thickness as $\tau(x_a,x_b) = \int_{x_a}^{x_b} \kappa_t(x)dx$, the RTE accepts an integral form which at a point x_a reads

$$
L(x_a,\vec{\omega}) = e^{-\tau(x_a,x_b)}L_b(x_b,\vec{\omega}) + L_m(x_a,x_b,\vec{\omega}) \tag{2}
$$

$$
L_m(x_a,x_b,\vec{\omega}) = \int_{x_a}^{x_b} e^{-\tau(x_a,x)}(\kappa_a(x)L_e(x,\vec{\omega}) + \kappa_s(x)L_i(x,\vec{\omega}))dx.
$$

Assuming a homogeneous non-emitting medium of phase function Φ with argument the angle ϕ illuminated by an anisotropic point light source of intensity I located at position $\vec{p}_l$ and parameterized by the angle θ with the normalized direction $\vec{v}_l$, the in-scattered radiance formulated in [14] can be extended to a point $\vec{p}_e + x\vec{v}_e$ along the view ray of origin $\vec{p}_e$ and direction $\vec{v}_e$ as

$$
L_i(x,\vec{\omega}) = \frac{e^{-\kappa_t d(x,\vec{\omega})}}{d(x,\vec{\omega})^2} I\left(\arccos\left(\frac{(\vec{p}_e + x\vec{v}_e - \vec{p}_l)\cdot\vec{v}_l}{d(x,\vec{\omega})}\right)\right)\Phi(\phi(x,\vec{\omega})) \tag{3}
$$

where the distance from the light source to the point is defined as $d(x,\vec{\omega}) = \sqrt{h^2 + (x - x_h)^2}$, and where h is the distance from the light to the ray and x_h the coordinate of its projection onto it,

both being constant for a given orientation as illustrated in figure 1. Defining $d_{el} = \vec{v}_e \cdot \vec{v}_l$ and $d_{lel} = (\vec{p}_e - \vec{p}_l)\cdot\vec{v}_l$, and using a 3-variate interval notation specifying the lower endpoint, light projection coordinate and upper endpoint respectively of the space of integration, equation 2 then reads the following where $x \in (-\infty, x_h, \infty)$

$$
L(x_a,\vec{\omega}) = e^{-\kappa_t(x_b - x_a)}L_b(x_b,\vec{\omega}) + L_m(x_a,x_b,\vec{\omega})
$$

$$
L_m(x_a,x_b,\vec{\omega}) = \kappa_s e^{\kappa_t x_a}\int_{x_a}^{x_b}\frac{e^{-\kappa_t\left(x + \sqrt{h^2 + (x - x_h)^2}\right)}}{h^2 + (x - x_h)^2} \tag{4}
$$

$$
I\left(\arccos\left(\frac{d_{el}x + d_{lel}}{\sqrt{h^2 + (x - x_h)^2}}\right)\right)\Phi\left(\arctan\left(\frac{x - x_h}{h}\right) + \frac{\pi}{2}\right)dx.
$$

3.2 Simplified Formulation

As in [15], we start by simplifying the formulation of the medium radiance via the change of variable $u = \frac{x - x_h}{h}$ with $u \in (-\infty, 0, \infty)$ mapping coordinates before x_h to negative values and that beyond x_h to positive ones. Defining the optical distance from the light to the ray as $H = \kappa_t h$ and the constant $d_c = \frac{d_{el}x_h + d_{lel}}{h}$ then yields

$$
L_m(x_a,x_b,\vec{\omega}) = \frac{\kappa_s}{h}e^{\kappa_t(x_a - x_h)}\int_{\frac{x_a - x_h}{h}}^{\frac{x_b - x_h}{h}}\frac{e^{-H(u + \sqrt{1 + u^2})}}{1 + u^2} \tag{5}
$$

$$
I\left(\arccos\left(\frac{d_{el}u + d_c}{\sqrt{1 + u^2}}\right)\right)\Phi\left(\arctan(u) + \frac{\pi}{2}\right)du.
$$

We also note that almost all phase functions are expressed in terms of the cosine of the angle and define Φ_c such that $\Phi(\phi) = \Phi_c(\cos(\phi))$. Without loss of generality, the same assumption is made about the light distribution and we define I_c such that $I(\theta) = I_c(\cos(\theta))$. Plugging this into equation 5 gives

$$
L_m(x_a,x_b,\vec{\omega}) = \frac{\kappa_s}{h}e^{\kappa_t(x_a - x_h)}\int_{\frac{x_a - x_h}{h}}^{\frac{x_b - x_h}{h}}\frac{e^{-H(u + \sqrt{1 + u^2})}}{1 + u^2} \tag{6}
$$

$$
I_c\left(\frac{d_{el}u + d_c}{\sqrt{1 + u^2}}\right)\Phi_c\left(-\frac{u}{\sqrt{1 + u^2}}\right)du.
$$

In this work, the impact of the medium on surface shading is assumed to be dominated by extinction phenomena and the background radiance is therefore computed as follows

$$
L_b(x_b,\vec{\omega}) = \frac{e^{-\kappa_t d(x_b,\vec{\omega})}}{d(x_b,\vec{\omega})^2}I_c(-\vec{\omega}_i \cdot \vec{v}_l)\beta(\vec{\omega},\vec{\omega}_i,\vec{n})\,\vec{\omega}_i\cdot\vec{n}, \tag{7}
$$

where $\vec{n}$ is the surface normal at x_b, $\vec{\omega}_i$ is a vector directed towards the light source and β is the bidirectional reflectance distribution function (BRDF). The evaluation of the medium radiance is addressed in the remainder of this document.

3.3 First Analytical Reformulation

Following the substitution proposed in [15], we define $v = u + \sqrt{1 + u^2}$ where $v \in (0, 1, \infty)$ which yields

$$
L_m(x_a,x_b,\vec{\omega}) = \frac{\kappa_s}{h}e^{\kappa_t(x_a - x_h)}2\int_{v_a}^{v_b}\frac{e^{-Hv}}{v^2 + 1} \tag{8}
$$

$$
I_c\left(\frac{d_{el}(v^2 - 1) + 2d_cv}{v^2 + 1}\right)\Phi_c\left(-\frac{v^2 - 1}{v^2 + 1}\right)dv
$$

where we note $v_a = v(x_a)$ and $v_b = v(x_b)$ with

$$
v(x) = \frac{x - x_h}{h} + \sqrt{1 + \left(\frac{x - x_h}{h}\right)^2}. \tag{9}
$$

Since deriving a custom analytical solution for all existing phase functions and light distributions is obviously impossible, we also use an expansion into a Taylor series as to express any phase function and light distribution as a polynomial, hence providing a common generic representation. Doing so yields $I_c\Phi_c = \sum_{n=0}^{N-1} c_n v^n$ and equation 8 then becomes

$$L_m(x_a,x_b,\vec{\omega}) = \frac{\kappa_s}{h} e^{\kappa_t(x_a-x_h)} 2 \sum_{n=0}^{N-1} c_n \int_{v_a}^{v_b} \frac{e^{-Hv}}{v^2+1} v^n \, dv. \quad (10)$$

While referring the reader to [15] for the details of the derivation, we define the imaginary entity $\iota^2 = -1$ and Ei as the exponential integral function [1], and recall the notations $I_0(a,v_a,v_b) = i_0(a,v_b) - i_0(a,v_a)$ and $I_1(a,v_a,v_b) = i_1(a,v_b) - i_1(a,v_a)$ with

$$i_0(a,v) = \sin(a)\Re(Ei(av+\iota a)) - \cos(a)\Im(Ei(av+\iota a)) \quad (11)$$
$$i_1(a,v) = \cos(a)\Re(Ei(av+\iota a)) + \sin(a)\Im(Ei(av+\iota a)).$$

The solution to equation 10 then reads

$$L_m(x_a,x_b,\vec{\omega}) = \frac{\kappa_s}{h} e^{\kappa_t(x_a-x_h)} 2 \sum_{n=0}^{N-1} c_n \left((-1)^{\lfloor \frac{n}{2} \rfloor} I_{(n \bmod 2)}(-H,v_a,v_b) \right.$$
$$\left. + \sum_{j=0}^{n-2} \left(e^{-Hv_b} v_b^j - e^{-Hv_a} v_a^j \right) c(-H,j,n) \right) \quad (12)$$

where

$$c(a,j,n) = \sum_{\substack{i=(n-2-j) \bmod 2 \\ i+=2}}^{n-2-j} (-1)^{\frac{n-i-j}{2}} \frac{(i+j)!}{j!} \left(-\frac{1}{a} \right)^{i+1}. \quad (13)$$

Because the expansion is expressed in terms of powers of the variable of integration, the series will converge rapidly whenever the magnitude of the latter is no greater than 1 and slowly otherwise. Given the space of the variable v, the reformulation derived above consequently yields quick convergence with a few terms on the first half of the domain while requiring many terms on the second half.

3.4 Second Analytical Reformulation
We now define a complementary reformulation and propose the substitution $w = u - \sqrt{1+u^2}$ with $w \in (-\infty,-1,0)$ which yields

$$L_m(x_a,x_b,\vec{\omega}) = \frac{\kappa_s}{h} e^{\kappa_t(x_a-x_h)} 2 \int_{w_a}^{w_b} \frac{e^{\frac{H}{w}}}{w^2+1} \quad (14)$$
$$I_c \left(-\frac{d_{el}(w^2-1)+2d_c w}{w^2+1} \right) \Phi_c \left(\frac{w^2-1}{w^2+1} \right) dw$$

where we note $w_a = w(x_a)$ and $w_b = w(x_b)$ with

$$w(x) = \frac{x-x_h}{h} - \sqrt{1 + \left(\frac{x-x_h}{h} \right)^2}. \quad (15)$$

Expanding the phase function and light distribution into a Taylor series yields $I_c\Phi_c = \sum_{n=0}^{N-1} d_n w^n$ and equation 14 then becomes

$$L_m(x_a,x_b,\vec{\omega}) = \frac{\kappa_s}{h} e^{\kappa_t(x_a-x_h)} 2 \sum_{n=0}^{N-1} d_n \int_{w_a}^{w_b} \frac{e^{\frac{H}{w}}}{w^2+1} w^n \, dw. \quad (16)$$

While appendix A provides the details of the derivation, we define $J_0(a,w_a,w_b) = j_0(a,w_b) - j_0(a,w_a)$, $J_1(a,w_a,w_b) = j_1(a,w_b) - j_1(a,w_a)$ and $J_e(a,w_a,w_b) = Ei\left(\frac{a}{w_b}\right) - Ei\left(\frac{a}{w_a}\right)$ with

$$j_0(a,w) = -\sin(a)\Re\left(Ei\left(\frac{a}{w}+\iota a\right) \right) + \cos(a)\Im\left(Ei\left(\frac{a}{w}+\iota a\right) \right) \quad (17)$$
$$j_1(a,w) = \cos(a)\Re\left(Ei\left(\frac{a}{w}+\iota a\right) \right) + \sin(a)\Im\left(Ei\left(\frac{a}{w}+\iota a\right) \right) - Ei\left(\frac{a}{w}\right).$$

The solution to equation 16 finally reads

$$L_m(x_a,x_b,\vec{\omega}) = \frac{\kappa_s}{h} e^{\kappa_t(x_a-x_h)} 2 \sum_{n=0}^{N-1} d_n \left((-1)^{\lfloor \frac{n}{2} \rfloor} J_{(n \bmod 2)}(H,w_a,w_b) \right. \quad (18)$$
$$\left. +J_e(H,w_a,w_b) \, H \, d(H,0,n) - \sum_{j=0}^{n-2} \left(e^{\frac{H}{w_b}} w_b^{j+1} - e^{\frac{H}{w_a}} w_a^{j+1} \right) d(H,j,n) \right)$$

where

$$d(a,j,n) = \sum_{\substack{i=(n-2-j) \bmod 2 \\ i+=2}}^{n-2-j} (-1)^{\frac{n-i-j}{2}} \frac{j!}{(i+j+1)!} a^i. \quad (19)$$

Because the space of the variable w exhibits properties that are complementary to that of the variable from the previous section, the reformulation derived above converges quickly on the second half of the domain while requiring many terms on the first half.

3.5 Combined Formulation
In order for the Taylor expansions to converge rapidly over the entire domain, each reformulation is used over its finite semi-interval such that the variable of integration always has a magnitude smaller than 1. Therefore, considering the simplified formulation given in equation 6, the first reformulation is used if both bounds of the domain of integration are negative, while the second is used if both are positive. In case the bounds have opposite signs, the integral is split into 2 sub-integrals, each being estimated separately depending on the sign of its upper bound. If the latter is negative, the first reformulation is used with a lower bound of 1, while the second reformulation is used with a lower bound of -1 if it is positive.

$$L_m(x_a,x_b,\vec{\omega}) = L_m(x_h,x_b,\vec{\omega}) - L_m(x_h,x_a,\vec{\omega}) = \frac{\kappa_s}{h} e^{\kappa_t(x_a-x_h)} \quad (20)$$
$$\left(\int_0^{\frac{x_b-x_h}{h}} \frac{e^{-H(u+\sqrt{1+u^2})}}{1+u^2} I_c\left(\frac{d_{el}u+d_c}{\sqrt{1+u^2}} \right) \Phi_c\left(-\frac{u}{\sqrt{1+u^2}} \right) du - \right.$$
$$\left. \int_0^{\frac{x_a-x_h}{h}} \frac{e^{-H(u+\sqrt{1+u^2})}}{1+u^2} I_c\left(\frac{d_{el}u+d_c}{\sqrt{1+u^2}} \right) \Phi_c\left(-\frac{u}{\sqrt{1+u^2}} \right) du \right).$$

Although it might at first seem like a separate Taylor series is required for each reformulation, the simple change of sign of the cosine parameter between both representations actually makes the correspondence between their respective expansions fairly trivial. For even functions such as a Rayleigh phase function or a raising to an even exponent as used to define a two-lobed spotlight distribution, the two series of derivatives are actually identical and a single expansion is therefore necessary. When considering a Henyey-Greenstein phase function, the change of sign of the parameter is essentially equivalent to a change of sign of the asymmetry coefficient, and here again, a single expansion is effectively sufficient.

Also, as the phase function parameter only depends on the variable of integration, the coefficients can be computed once only from an expansion in a fixed point, typically $\frac{1}{2}$ for the first reformulation and $-\frac{1}{2}$ for the second. However, the light distribution parameter also depends on external factors and the coefficients must consequently be recomputed from the sequence of derivatives for each individual view ray. We therefore propose to expand the function in the mid-point of the given domain of integration, hence yielding more accurate results at virtually no additional cost.

4 IMPLEMENTATION
This section starts by addressing the implementation of the complex-valued and real-valued exponential integral respectively. A discussion of the evaluation of the introduced functions is then presented before providing a pseudo-code illustration summarizing the various steps involved in the overall algorithm.

4.1 Complex-Valued Exponential Integral

An efficient implementation for optically thin media was provided in [15] which allows for both a relative and an absolute control on the precision of the results. However, this implementation is solely based on the power series representation of the complex exponential integral which converges slowly in optically thick media, eventually leading to numerical instabilities. As the exponential integral belongs to the class of non-elementary special functions and is not part of the standard $C/C++$ libraries, we here provide a more robust implementation that additionally relies on the asymptotic series representation, albeit only allowing for a control on the absolute error of the results.

Assuming $z \notin (-\infty, 0]$, the convergent power series reads

$$Ei(z) = \gamma + \ln(z) + \sum_{k=1}^{\infty} \frac{z^k}{k\,k!} \tag{21}$$

where the Euler-Mascheroni constant is defined as $\gamma \approx 0.5772156649015328606065112\ldots$ [1]. Formulating a complex number $z = x + \iota y$ into its exponential form $z = \rho e^{\iota \varphi}$ where $\rho = |z| = \sqrt{x^2 + y^2}$ and $\varphi = Arg(z) = atan2(y,x)$ gives

$$\Re(Ei(z)) = \gamma + \ln(\rho) + \sum_{k=1}^{\infty} \frac{\rho^k}{k\,k!} \cos(k\varphi) \tag{22}$$

$$\Im(Ei(z)) = \varphi + \sum_{k=1}^{\infty} \frac{\rho^k}{k\,k!} \sin(k\varphi). \tag{23}$$

Assuming $z \notin (-\infty, \infty)$, the divergent asymptotic series reads

$$Ei(z) \approx e^z \sum_{k=1}^{K} \frac{k!}{k\,z^k} + \iota\, sign(\Im(z))\pi \tag{24}$$

where $K = \lfloor \rho \rfloor + 1$ and from which follows that

$$\Re(Ei(z)) \approx e^x \sum_{k=1}^{K} \frac{k!}{k\,\rho^k} cos(y - k\varphi) \tag{25}$$

$$\Im(Ei(z)) \approx e^x \sum_{k=1}^{K} \frac{k!}{k\,\rho^k} sin(y - k\varphi) + sign(y)\pi. \tag{26}$$

As the asymptotic series imposes a bound on the achievable accuracy for a given z, the choice of the series to be used to reach a well defined precision requirement is a crucial factor. Since the definition of such criterion was however absent from all the literature that we could consult, we derived a rule on our own based on a mathematical analysis of the behavior of the asymptotic series. As the derivation of this criterion is well beyond the scope of the current document, we readily report our result below which reads

$$1 \leq \rho \quad \wedge \quad x - \lfloor \rho \rfloor < ln(\varepsilon) - 1 \tag{27}$$

where the term on the right-hand side of the second inequation is constant for a given tolerable absolute error ε. If the condition is satisfied the asymptotic series should be used while the power series should be preferred otherwise. Given that the complex exponential integral is at the heart of our approach, pseudo-code for its evaluation based on the preceding formulations is provided in figure 2.

4.2 Real-Valued Exponential Integral

Regarding the real-valued exponential integral appearing in the definition of J_e, we note that the parameters are here always negative. Given that $Ei(-x) = -E_1(x)$ for $x > 0$ with E_1 being the Theis well function, the approximations available to the latter [1] can be used and are recalled below for completeness purposes.

```
1.  Ei(x, y, precision, maxIterations)
2.    ρ = sqrt(x*x + y*y);
3.    φ = atan2(y,x);
4.    if(1 ≤ ρ && x − floor(ρ) < log(precision) − 1)
5.      eix = 0;
6.      eiy = (0 < y) ? PI : − PI;
7.      term = exp(x)/ρ;
8.      maxIterations = min(maxIterations, floor(ρ) + 1);
9.      for(k = 1; k ≤ maxIterations; k++)
10.       angle = y − k*φ;
11.       eix+ = term*cos(angle);
12.       eiy+ = term*sin(angle);
13.       if(term < precision)break;
14.       term* = k/ρ;
15.   else
16.     eix = γ + log(ρ);
17.     eiy = φ;
18.     powfac = 1;
19.     for(k = 1; k ≤ maxIterations; k++)
20.       powfac* = ρ/k;
21.       term = powfac/k;
22.       angle = k*φ;
23.       eix+ = term*cos(angle);
24.       eiy+ = term*sin(angle);
25.       if(term < precision)break;
26.   return (eix, eiy);
```

Figure 2: Pseudo-code for evaluating the Exponential Integral in the complex plane excluding the real axis

For $0 < x \leq 1$, the following polynomial approximation exhibits $|\varepsilon(x)| < 2 \cdot 10^{-7}$

$$E_1(x) = a_0 + a_1 x + a_2 x^2 + a_3 x^3 + a_4 x^4 + a_5 x^5 - ln(x) + \varepsilon(x) \tag{28}$$

$$\begin{array}{ll} a_0 = -0.57721566 & a_3 = +0.05519968 \\ a_1 = +0.99999193 & a_4 = -0.00976004 \\ a_2 = -0.24991055 & a_5 = +0.00107857 \end{array} \tag{29}$$

For $1 < x < \infty$, the rational approximation yields $|\varepsilon(x)| < 2 \cdot 10^{-8}$

$$E_1(x) = \frac{e^{-x}}{x} \left(\frac{a_0 + a_1 x + a_2 x^2 + a_3 x^3 + x^4}{b_0 + b_1 x + b_2 x^2 + b_3 x^3 + x^4} + \varepsilon(x) \right) \tag{30}$$

$$\begin{array}{ll} a_0 = 0.2677737343 & b_0 = 3.9584969228 \\ a_1 = 8.6347608925 & b_1 = 21.0996530827 \\ a_2 = 18.0590169730 & b_2 = 25.6329561486 \\ a_3 = 8.5733287401 & b_3 = 9.5733223454 \end{array} \tag{31}$$

4.3 Functions I_0, I_1, J_0, J_1 and J_e

We now highlight the identities below

$$j_0(a,w) = -i_0\left(a, \frac{1}{w}\right) \tag{32}$$

$$j_1(a,w) = i_1\left(a, \frac{1}{w}\right) - Ei\left(\frac{a}{w}\right) \tag{33}$$

from which follows that

$$J_0(a, w_a, w_b) = -I_0\left(a, \frac{1}{w_a}, \frac{1}{w_b}\right) \tag{34}$$

$$J_1(a, w_a, w_b) = I_1\left(a, \frac{1}{w_a}, \frac{1}{w_b}\right) - J_e(a, w_a, w_b). \tag{35}$$

Given the recurrence of functions I_0 and I_1, pseudo-code for their evaluation based on the implementation of the exponential integral previously presented is provided in figure 3 which can be readily used in place of the implementation from [15].

1. **I01(a, va, vb, precision, maxIterations)**
2. $(eix_a, eiy_a) = \text{Ei}(a * v_a, a, precision, maxIterations)$;
3. $(eix_b, eiy_b) = \text{Ei}(a * v_b, a, precision, maxIterations)$;
4. $eix_b \mathrel{-}= eix_a$;
5. $eiy_b \mathrel{-}= eiy_a$;
6. $cos_a = \cos(a)$;
7. $sin_a = \sin(a)$;
8. $I_0 = sin_a * eix_b - cos_a * eiy_b$;
9. $I_1 = cos_a * eix_b + sin_a * eiy_b$;
10. $return\ (I_0, I_1)$;

Figure 3: Pseudo-code for computing $I_0(a, v_a, v_b)$ and $I_1(a, v_a, v_b)$

It is also worth noting that the terms I_0 and I_1 in equation 12 and the terms J_0, J_1 and J_e in equation 18 are independent of the value of the iterator n and can consequently be computed once only before entering the loops.

4.4 Overall Algorithm

High-level pseudo-code summarizing the various steps involved in the overall algorithm is finally provided in figure 4. The coefficients of the Taylor expansions that appear on lines 6 and 11 can be computed using the series of derivatives provided in appendix B.

1. **ComputeEyeRadiance()**
2. Compute L_m;
3. Compute bounds of integral in equation 6;
4. If both are negative, use first reformulation;
5. Compute bounds v_a and v_b as in equation 9;
6. Compute coefficients c_n for arguments in equation 8;
7. Compute I_0 and I_1 as in section 4.3;
8. Compute L_m using equations 12 and 13;
9. If both are positive, use second reformulation;
10. Compute bounds w_a and w_b as in equation 15;
11. Compute coefficients d_n for arguments in equation 14;
12. Compute J_0, J_1 and J_e as in section 4.3;
13. Compute L_m using equations 18 and 19;
14. If they have opposite signs, use combined formulation;
15. Compute each sub-integral based on upper bound sign;
16. Compute L_m as in first part of equation 20;
17. Compute L_b as in equation 7;
18. Compute L as in first part of equation 4;

Figure 4: Pseudo-code of the overall algorithm

5 RESULTS

The method was first implemented in a software ray-tracer making use of the first 6 terms of the Taylor expansions. In order to assess the robustness of the combined formulation, we designed scenes with relatively wide extents of integration. Figure 5(a) illustrates the results obtained for a Rayleigh phase function and shows the limitations of the first analytical reformulation proposed in [15], while when combined with our second analytical reformulation, results become virtually indistinguishable from the reference solution. The extension of the first reformulation to anisotropic lights was also evaluated in figure 5(b) where artifacts are clearly visible while the new combined formulation proves to be fairly accurate.
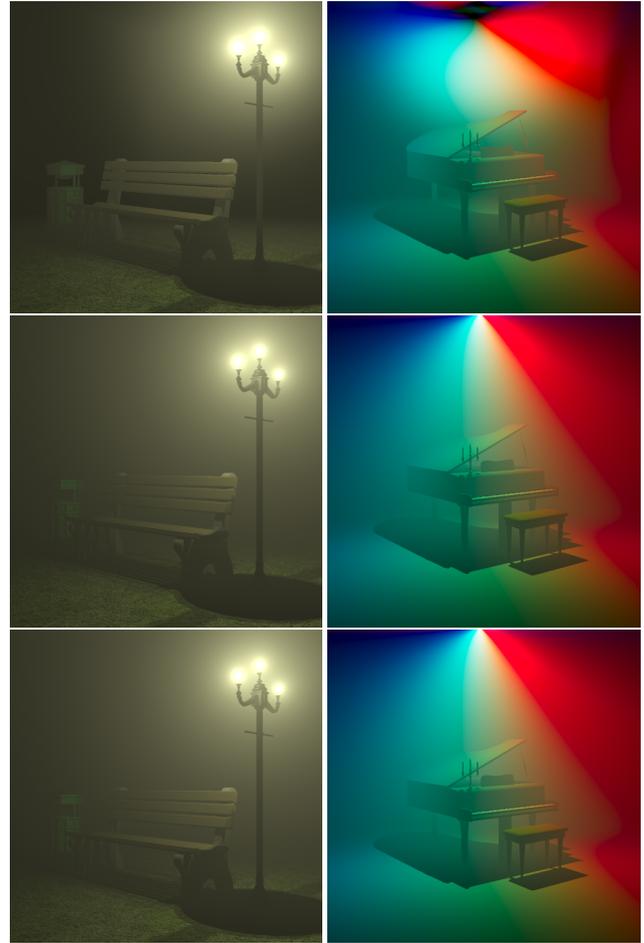

Figure 5: (a) A bench in a park covered in anisotropic mist, and (b) a concert stage lit by 3 colorful spotlights, rendered using (from top to bottom) the first analytical reformulation as proposed in [15], our combined formulation, and Monte Carlo integration.

Figure 6(a) shows the impact of the point of expansion for anisotropic sources. While plausible results are obtained by expanding the light distribution at fixed positions, artifacts remain such as an erroneous darkening above the streetlamp and inaccurate brightening around the car. On the other hand, a custom expansion in the mid-point of the bounds of each integral yields results matching the reference image more closely.

Finally, the method was implemented in a fragment shader using OpenGL and Cg running on an NVIDIA GeForce 8800 GTX under Windows XP 32-bit. The integral was evaluated independently for each color channel, hence 3 times per fragment, using the first 4 terms of the Taylor expansions due to hardware-specific limitations. Figure 6(b) provides a comparison of the performance characteristics for a scene containing an optically thick medium with an isotropic phase function and light source. While rendering at 70 FPS in about 33 iterations, the implementation provided in [15] leads to numerical instabilities inducing exceptional floating-point values, e.g. NaN or Inf, here flagged as saturated pixels. In contrast, our new implementation proves to be much more robust and yields a frame rate of 226 FPS while converging in about 23 iterations. Performance characteristics for anisotropic light sources were also evaluated and despite the extra computation involved, interactivity was maintained at 39 FPS.
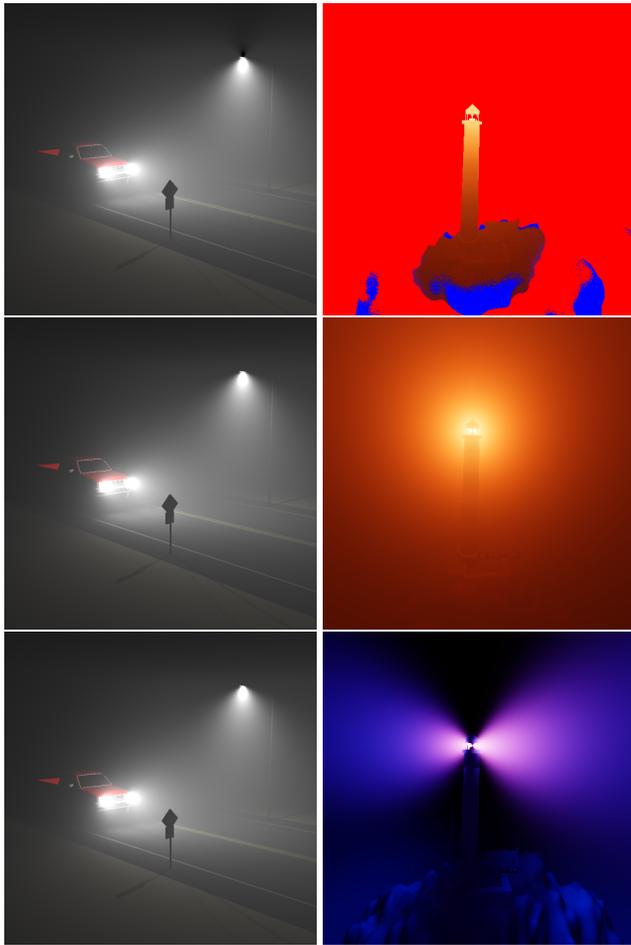
Figure 6: (a) A car driving on a foggy road illuminated by anisotropic headlights and a streetlamp, rendered using (from top to bottom) our combined formulation with an expansion in a fixed point, our combined formulation with an expansion in the mid-point of the integration domain, and Monte Carlo integration. (b) A lighthouse in thick brume rendered in real-time using (from top to bottom) an isotropic light with the implementation from [15] compared against our numerically stable implementation, and an anisotropic two-lobed spotlight.

6 DISCUSSION AND FUTURE WORK

While the proposed combined formulation substantially increases the accuracy of the method, relying on a Taylor expansion induces inherent limitations. Besides the need for human intervention, many terms are required to accurately model functions with high frequency features, and strongly peaked phase functions or very focused light beams are problematic in practice.

In addition to the coupling with a shadow volume algorithm to render light shafts as in [2], the extension to inhomogeneous media could also be addressed as to make the method suitable to a broader spectrum of applications, and the impact of in-scattering on surface shading considered as in [18] in order to increase realism.

7 CONCLUSION

In this paper, we have presented a novel analytical approach to single scattering from point light sources in homogeneous media. We have shown how to derive a combined formulation of the airlight integral providing more accurate evaluations of anisotropic phase functions and which is, to the best of our knowledge, the first method to handle anisotropic light distributions analytically.

The technique relies neither on precomputation nor on storage, and we have provided a practical implementation yielding numerically stable results more efficiently. Moreover, the adequacy of the method to graphics hardware was illustrated and its suitability to real-time applications demonstrated.

REFERENCES

[1] M. Abramowitz and I. A. Stegun. *Handbook of Mathematical Functions with Formulas, Graphs, and Mathematical Tables*. U.S. Department of Commerce, 1972.

[2] V. Biri, D. Arquès, and S. Michelin. Real Time Rendering of Atmospheric Scattering and Volumetric Shadows. *Journal of WSCG*, 14:65–72, 2006.

[3] V. Biri, S. Michelin, and D. Arquès. Real-Time Single Scattering with Shadows, 2003.

[4] J. F. Blinn. Light Reflection Functions for Simulation of Clouds and Dusty Surfaces. *SIGGRAPH Computer Graphics*, 16(3):21–29, 1982.

[5] E. Cerezo, F. Perez-Cazorla, X. Pueyo, F. Seron, and F. Sillion. A Survey on Participating Media Rendering Techniques. *The Visual Computer*, 21(5):303–328, 2005.

[6] Y. Dobashi, T. Yamamoto, and T. Nishita. Interactive Rendering Method for Displaying Shafts of Light. In *Pacific Graphics*, pages 31–37, 2000.

[7] Y. Dobashi, T. Yamamoto, and T. Nishita. Interactive Rendering of Atmospheric Scattering Effects Using Graphics Hardware. In *Graphics Hardware*, pages 99–108, 2002.

[8] M. E. and S. T. Volume Light. NVIDIA White Paper, 2008.

[9] N. Hoffman and A. J. Preetham. Rendering Outdoor Light Scattering in Real Time. ATI White Paper, 2002.

[10] T. Imagire, H. Johan, N. Tamura, and T. Nishita. Anti-Aliased and Real-Time Rendering of Scenes with Light Scattering Effects. *Visual Computer*, 23(9):935–944, 2007.

[11] P. Lecocq, S. Michelin, D. Arquès, and A. Kemeny. Mathematical Approximation for Real-Time Lighting Rendering Through Participating Media. In *Pacific Graphics*, pages 400–401, 2000.

[12] N. L. Max. Atmospheric Illumination and Shadows. *SIGGRAPH*, 20(4):117–124, 1986.

[13] K. Mitchell. Volumetric Light Scattering as a Post-Process. In *GPU Gems 3*, chapter 13, pages 275–285. 2007.

[14] T. Nishita, Y. Miyawaki, and E. Nakamae. A Shading Model for Atmospheric Scattering Considering Luminous Intensity Distribution of Light Sources. *SIGGRAPH Comp. Graphics*, 21(4):303–310, 1987.

[15] V. Pegoraro and S. G. Parker. An Analytical Solution to Single Scattering in Homogeneous Participating Media. *Computer Graphics Forum (Proceedings of Eurographics)*, 28(2):(to appear), 2009.

[16] K. Riley, D. S. Ebert, M. Kraus, J. Tessendorf, and C. D. Hansen. Efficient Rendering of Atmospheric Phenomena. In *Eurographics Symposium on Rendering*, pages 375–386, 2004.

[17] R. Siegel and J. R. Howell. *Thermal Radiation Heat Transfer*. Hemisphere Publishing Corporation, 1981.

[18] B. Sun, R. Ramamoorthi, S. G. Narasimhan, and S. K. Nayar. A Practical Analytic Single Scattering Model for Real Time Rendering. *Transactions on Graphics*, 24(3):1040–1049, 2005.

[19] P. J. Willis. Visual Simulation of Atmospheric Haze. *Computer Graphics Forum*, 6(1):35–42, 1987.

[20] C. Wyman and S. Ramsey. Interactive Volumetric Shadows in Participating Media with Single-Scattering. In *Symposium on Interactive Ray Tracing*, pages 87–92, 2008.

A ANTIDERIVATIVES

As an antiderivative for the resulting integrand did not appear in any of the standard tables of integrals we had access to, we derived a solution on our own and provide this potentially new result below

$$\int \frac{e^{\frac{a}{w}}}{w^2+1} w^n dw = Ei\left(\frac{a}{w}\right) a\, d(a,0,n) - e^{\frac{a}{w}} \sum_{j=0}^{n-2} w^{j+1} d(a,j,n) + \frac{1}{2} \quad (36)$$

$$\left(\imath^{n-1} e^{-\imath a} Ei\left(\frac{a}{w}+\imath a\right) + \frac{1}{\imath^{n-1}} e^{\imath a} Ei\left(\frac{a}{w}-\imath a\right) - \left(\imath^{n-1}+\frac{1}{\imath^{n-1}}\right) Ei\left(\frac{a}{w}\right) \right).$$

In order to express formula 36 in terms of real entities, we introduce two other antiderivatives. Noting that $Ei(\bar{z}) = \overline{Ei(z)}$ and expanding each term into its real $\Re$ and imaginary $\Im$ parts, these simplify into functions that we referred to as j_0 and j_1 respectively

$$\int \frac{e^{\frac{a}{w}}}{w^2+1} dw = -\frac{\imath}{2}\left(e^{-\imath a} Ei\left(\frac{a}{w}+\imath a\right) - e^{\imath a} Ei\left(\frac{a}{w}-\imath a\right)\right)$$
$$= j_0(a,w) \quad (37)$$

$$\int \frac{e^{\frac{a}{w}}}{w^2+1} w\, dw = \frac{1}{2}\left(e^{-\imath a} Ei\left(\frac{a}{w}+\imath a\right) + e^{\imath a} Ei\left(\frac{a}{w}-\imath a\right)\right) - Ei\left(\frac{a}{w}\right)$$
$$= j_1(a,w). \quad (38)$$

Exploiting the periodicity of $\imath^{n-1}$, it then follows that

$$\int \frac{e^{\frac{a}{w}}}{w^2+1} w^n dw = (-1)^{\lfloor \frac{n}{2}\rfloor} j_{(n \bmod 2)}(a,w)$$
$$+ Ei\left(\frac{a}{w}\right) a\, d(a,0,n) - e^{\frac{a}{w}} \sum_{j=0}^{n-2} w^{j+1} d(a,j,n). \quad (39)$$

B TAYLOR SERIES COEFFICIENTS

We finally provide series of derivatives for sample anisotropic functions which can be readily used to compute the coefficients of the Taylor representations. Considering a Rayleigh phase function, the first 6 terms of the expansion are described by

$$f^{(0)}(x) = \frac{3}{4}\left(1+\left(\mp\frac{x^2-1}{x^2+1}\right)^2\right) = \frac{3}{4}\frac{2}{(x^2+1)^2}(x^4+1)$$

$$f^{(1)}(x) = \frac{3}{4}\frac{2^2}{(x^2+1)^3} 2(x^3-x)$$

$$f^{(2)}(x) = \frac{3}{4}\frac{2^3}{(x^2+1)^4}(-3x^4+8x^2-1) \quad (40)$$

$$f^{(3)}(x) = \frac{3}{4}\frac{2^4}{(x^2+1)^5} 6(x^5-5x^3+2x)$$

$$f^{(4)}(x) = \frac{3}{4}\frac{2^5}{(x^2+1)^6} 3(-5x^6+40x^4-33x^2+2)$$

$$f^{(5)}(x) = \frac{3}{4}\frac{2^6}{(x^2+1)^7} 15(3x^7-35x^5+49x^3-9x).$$

Using the short-hand notation $a=d_{el}$ and $b=2d_c$, the following series describes the first 4 terms of a two-lobed light distribution which raises the cosine parameter to an even power p, and reads

$$f^{(0)}(x) = \left(\pm\frac{a(x^2-1)+bx}{x^2+1}\right)^p = \frac{(a(x^2-1)+bx)^p}{(x^2+1)^p}$$

$$f^{(1)}(x) = \frac{(a(x^2-1)+bx)^{p-1}}{(x^2+1)^{p+1}} p\left(4ax-b(x^2-1)\right) \quad (41)$$

$$f^{(2)}(x) = \frac{(a(x^2-1)+bx)^{p-2}}{(x^2+1)^{p+2}} p\left(4\left(-3x^4+4px^2-1\right)a^2\right.$$
$$\left. +2bx\left(x^4-6x^2-4p(x^2-1)+1\right)a+b^2\left(x^4-4x^2+p(x^2-1)^2-1\right)\right)$$

$$f^{(3)}(x) = \frac{(a(x^2-1)+bx)^{p-3}}{(x^2+1)^{p+3}} p$$
$$\left(16\left(4p^2x^3+(3x^4+5)x^3-3p(3x^5+x)\right)a^3\right.$$
$$-6b\left(x^8-14x^6+8x^4+8p^2(x^2-1)x^2-10x^2\right.$$
$$\left.+p(-10x^6+30x^4-6x^2+2)-1\right)a^2$$
$$-6b^2x\left(x^6-11x^4+3x^2-2p^2(x^2-1)^2+p(x^6-9x^4+15x^2+1)-1\right)a$$
$$\left.+b^3\left(-2x^6+18x^4+6x^2-p^2(x^2-1)^3-3p(x^6-5x^4+3x^2+1)+2\right)\right).$$

The derivatives yield the coefficients of the truncated power series centered in x_0. The polynomial coefficients can then be computed in-place from the latter in order of increasing index n by use of the binomial theorem to finally yield c_n or d_n as follows

$$c_n|d_n = \frac{1}{4\pi}\frac{1}{n!} \sum_{m=0}^{N-1-n} f^{(m+n)}(x_0)\frac{(-x_0)^m}{m!}. \quad (42)$$